

# Lagrangian statistics in turbulent channel flow

Jung-Il Choi,<sup>a)</sup> Kyongmin Yeo, and Changhoon Lee<sup>b)</sup>

*Department of Mechanical Engineering and Yonsei Center for Clean Technology, Yonsei University, 134 Shinchon-dong, Seodaemun-gu Seoul 120-749, Korea*

(Received 20 February 2003; accepted 14 November 2003; published online 4 February 2004)

The Lagrangian dispersion of fluid particles in inhomogeneous turbulence is investigated by a direct numerical simulation of turbulent channel flow. Lagrangian velocity and acceleration along a particle trajectory are computed by employing several interpolation schemes. Among the schemes tested, the four-point Hermite interpolation in the homogeneous directions combined with Chebyshev polynomials in the wall-normal direction seems to produce most reliable Lagrangian statistics. Inhomogeneity of Lagrangian statistics in turbulent boundary layer is investigated by releasing many particles at several different wall-normal locations and tracking those particles. The fluid particle dispersion and Lagrangian structure function of velocity are investigated for the Kolmogorov similarity. The behavior of the Lagrangian integral time scales, Kolmogorov constants  $a_0$  and  $C_0$  of the velocity structure function near the wall are discussed. The intermittent behavior of the fluid particle acceleration is also examined by kurtosis of the Lagrangian structure function. Finally, the effect of the initial particle location on the dispersion is analyzed by the probability density function of particle position at several downstream locations. © 2004 American Institute of Physics. [DOI: 10.1063/1.1644576]

## I. INTRODUCTION

One of the most interesting approaches for the turbulent study is the investigation of turbulent flows in Lagrangian frame. An issue of primary importance for the Lagrangian dispersion of fluid particles in turbulent flow concerns understanding of underlying turbulent physics and the development of the statistical models.<sup>1–8</sup> Past researches focused on Lagrangian statistics closely related with turbulent flow. Yet little is known regarding the fluid particle dispersion in a wall-bounded flow. It remains still unclear how to relate the presence of the wall to anisotropy and inhomogeneity of Lagrangian statistics.

The wall-bounded turbulent flow at low or moderate Reynolds number is well resolved by direct numerical simulation (DNS) of the Navier–Stokes equations, since all essential scales of turbulent motions are resolved. A critical part of the calculation in particle tracking is application of interpolation to obtain particle velocity from the known values of the Eulerian velocity fields<sup>9</sup> because the instantaneous position of a particle does not coincide with a computational grid point. Yeung and Pope<sup>10</sup> designed TS13, which is a third-order accurate, thirteen points, interpolation scheme, and applied it to isotropic turbulence to extract Lagrangian statistics. Balachandar and Maxey<sup>11</sup> also presented Lagrangian statistics by using several algorithms including a partial Hermite interpolation scheme. Kontomaris *et al.*<sup>9</sup> computed the fluid particle velocities in turbulent channel flow with combined interpolation schemes which consist of sixth-order

Lagrange polynomials or the Hermite schemes in homogeneous directions and Chebyshev polynomials in the wall-normal direction. In the present work, we have re-evaluated the accuracy of various interpolation schemes in DNS of turbulent channel flow and focused on the effect of the interpolation schemes on high-order Lagrangian statistics such as acceleration correlations.

A literature survey reveals that many numerical and experimental studies have been performed to examine the Lagrangian statistics of fluid particle dispersion in isotropic turbulence.<sup>4–7,12–14</sup> They have focused on the examination of Lagrangian time series in relation to Lagrangian stochastic model. The major question in stochastic modeling is how to implement inhomogeneity and anisotropy of near-wall flow and the effect of Reynolds number into models. In an effort to overcome inefficiency of the first-order stochastic model (stochastic model for the Lagrangian velocity increment) in representing anisotropy or Reynolds number effect, some proposed the second-order stochastic models for the increment of acceleration<sup>15,16</sup> within the context of the well-mixed class.<sup>17</sup>

Important elements in such approaches are specification of model constants  $C_0$  and  $a_0$ , which scale the velocity structure function in terms of the dissipation rate in the inertial range and the root-mean-square (rms) acceleration in terms of the dissipation rate and viscosity, respectively. According to the classical Kolmogorov scaling analysis,  $C_0$  and  $a_0$  are universal.<sup>2</sup> Recently, Yeung<sup>8</sup> suggested that the constant  $a_0$  for low Reynolds number flows is not universal and rather increasing as  $R_\lambda^{1/2}$  where  $R_\lambda$  is the Taylor-scale Reynolds number. Recently, La Porta *et al.*<sup>7,14</sup> reported similar trend in their experiments. Vedula and Yeung<sup>13</sup> provided further evidence to claim that the acceleration is dominated by

<sup>a)</sup>Present address: Center for Environmental Medicine, Asthma and Lung Biology, University of North Carolina at Chapel Hill, Chapel Hill, NC 27599-7310.

<sup>b)</sup>Electronic mail: cleee@yonsei.ac.kr

pressure gradients, which are highly intermittent and concentrated at intermediate scales in the turbulent spectrum, thus  $a_0$  deviating from the Kolmogorov scaling.

Direct estimate of  $C_0$ , which is essential in Lagrangian stochastic models of any order,<sup>17–20</sup> in either experiment or numerical simulation is difficult. Instead, the peak of the Lagrangian velocity structure function  $\langle \Delta v(\tau)^2 \rangle$  when normalized by the dissipation rate  $\epsilon$  and time span  $\tau$ , known as  $C_0^*$ , has been widely investigated. Yeung and Pope<sup>8</sup> have reported by using DNS that  $C_0^*$  has a strong dependence on Reynolds number in their low-Reynolds number simulations. Recent high-quality experiment<sup>6</sup> yielded  $C_0^* \sim 2.9$ . The discussion on the Kolmogorov constant has continued by a compilation of available experimental and numerical data,<sup>21</sup> delivering the uncertainty in the estimate of  $C_0$ . Since most works are restricted to isotropic flows, it is necessary first to characterize anisotropic nature of the Lagrangian statistics including the scaled velocity structure functions and acceleration correlations in near-wall turbulent flows.

For homogeneous shear flow with mean velocity some investigations were carried out in the Lagrangian framework.<sup>22,23</sup> It was reported that the Lagrangian auto-correlation of the streamwise velocity persists significantly longer than that of the other components. However, due to the non-stationary nature of the simulations, it is difficult to define the integral time scale of the velocity auto-correlations, thus preventing detailed investigation.

For the wall-bounded flow, the Lagrangian statistics have been studied for the investigation of transport mechanism,<sup>24,25</sup> for the evaluation of particle tracking algorithm,<sup>9</sup> and for the dispersion of particle tracers.<sup>26,27</sup> Using DNS, Iliopoulos and Hanratty<sup>28</sup> have studied point-source dispersion at a distance of 40 wall units from the wall in a fully developed channel flow for the evaluation of their stochastic model. Detailed statistics of Lagrangian quantities, however, have not been provided for anisotropic and inhomogeneous turbulent flow *near the wall*.

The main purpose of this study is to characterize the inhomogeneity of Lagrangian statistics in turbulent channel flow by using DNS. In our simulations, our strategy is to release many particles at the several wall-normal locations and then to track those particles to obtain the Lagrangian statistics. The inhomogeneity of fluid particle dispersion is discussed in the small-scale and inertial ranges. The auto-correlations of each component of the Lagrangian velocity and acceleration are obtained to examine near-wall inhomogeneity of dispersion. The classical Kolmogorov similarity hypothesis is applied to investigate the inhomogeneity and anisotropy of the universal constants  $a_0$  and  $C_0$ . Obviously, such information is very useful for the development of Lagrangian stochastic models of velocity<sup>17,18,29</sup> or of acceleration.<sup>16,20</sup> In addition to the analysis, the probability density function of the particle position is examined in the view from the inhomogeneity due to the different initial particle locations.

The paper is organized as follows: Numerical methods for direct numerical simulation will be briefly described in Sec. II; particle tracking algorithms are summarized in Sec. III; an assessment of the algorithms is presented in Sec. IV;

Lagrangian statistics are investigated in Sec. V; finally, concluding remarks are provided in Sec. VI.

## II. NUMERICAL SIMULATION

For an incompressible turbulent flow, the Navier–Stokes equations and continuity equation can be written as

$$\frac{\partial u_i}{\partial t} + \frac{\partial(u_i u_j)}{\partial x_j} = -\frac{\partial p}{\partial x_i} + \frac{1}{\text{Re}_\tau} \frac{\partial^2 u_i}{\partial x_j \partial x_j}, \quad (1)$$

$$\frac{\partial u_i}{\partial x_i} = 0, \quad (2)$$

where  $x_1$ ,  $x_2$ , and  $x_3$  are the streamwise, wall-normal and spanwise directions, respectively.  $u_i$  are the corresponding velocity components,  $p$  is the pressure normalized by  $\rho u_\tau^2$ , and  $\text{Re}_\tau$  is the Reynolds number,  $\text{Re}_\tau = u_\tau \delta / \nu$ . All variables are nondimensionalized by the wall-shear velocity  $u_\tau$ , and the channel half width  $\delta$ . Periodic boundary conditions are imposed in the streamwise and spanwise directions. The flow rate in the streamwise direction is kept constant.

Direct numerical simulations of turbulent channel flow at two Reynolds numbers ( $\text{Re}_\tau = 200$  and  $400$ ) are performed to investigate the Lagrangian statistics. Both a Chebyshev-tau method in the wall-normal direction and a dealiased Fourier method in the streamwise and spanwise directions are used. A semi-implicit time advancement scheme is employed by using the Crank–Nicolson implicit method for the viscous terms and an explicit third-order Runge–Kutta scheme for the nonlinear terms. The spectral numerical scheme used in this study is nearly the same as that used in Kim *et al.*<sup>30</sup> The domain size in the streamwise, wall-normal, and spanwise directions is (1256,400,418) wall units for  $\text{Re}_\tau = 200$  and (2513,800,837) wall units for  $\text{Re}_\tau = 400$ , respectively. The corresponding grids in each direction are  $64 \times 97 \times 64$  and  $128 \times 193 \times 128$ , respectively. For both Reynolds numbers,  $\Delta x^+ \approx 13$  and  $\Delta z^+ \approx 4$ , which are sufficient to resolve small-scale structures near the wall.<sup>31</sup>

The trace of a fluid particle is calculated by the numerical integration of the equation of particle motion, with the released particle position ( $\mathbf{x}_0$ ) at time  $t = 0$  as the initial condition:

$$\frac{d\mathbf{X}(t; \mathbf{x}_0)}{dt} = \mathbf{V}(t; \mathbf{x}_0), \quad (3)$$

where  $\mathbf{X}$  and  $\mathbf{V}$  are the position and the Lagrangian velocity of a fluid particle at time  $t$ , respectively. The instantaneous velocity of a fluid particle is the same as the Eulerian velocity at the position of the particle which generally does not coincide with the computational grid, i.e.,  $\mathbf{V}(t; \mathbf{x}_0) = \mathbf{U}(\mathbf{X}, t)$ . Therefore, the Lagrangian velocity should be numerically extracted from the nearest grid information using a proper interpolation scheme. To evaluate the algorithms, fluid particle velocity along a particle trajectory is computed by employing several schemes such as linear interpolation (Linear), sixth-order Lagrange polynomial interpolation (LG6CH) and the two-point and four-point Hermite interpolation schemes (HM2CH, HM4CH) in the homogeneous direction and Chebyshev polynomial in the wall-normal direc-

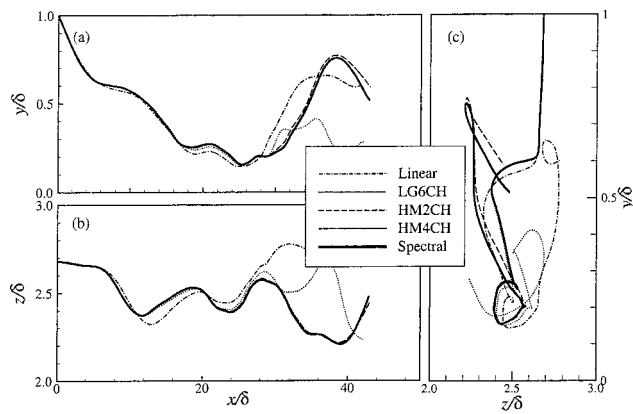


FIG. 1. Trajectories of a particle released at the center of channel using different interpolation schemes.

tion. The performance of the schemes is evaluated through comparison of errors in computed particle positions, velocities and accelerations against spectral interpolation (Spectral). A fluid particle is assigned with an initial position. This particle is then tracked by continually updating its position using the third-order Runge–Kutta time-advancement scheme.

### III. ASSESSMENT OF INTERPOLATION SCHEMES

In order to assess the several interpolation schemes before proceeding the investigation of Lagrangian statistics, we have simulated fluid particle dispersion in turbulent channel flow by using DNS. For the test of interpolation schemes, a fully developed channel flow at ( $Re_\tau=112$ ) using  $32 \times 65 \times 32$  grids in  $(4\pi, 2, 4\pi/3)\delta$  box is spectrally simulated.

Figure 1 shows trajectories of a fluid particle released at the center of the channel which were calculated by the aforementioned interpolation schemes. Three different plane views of the computed trajectories are shown in Fig. 1. The trajectories are initially identical and they remain reasonably close to each other until the particle reaches  $x/\delta=6$  [Figs. 1(a) and 1(b)]. The computed trajectory using Linear first begins to deviate from the exact spectral interpolation after  $x/\delta=6$ . The excursion of the trajectory obtained by LG6CH from that obtained by Spectral is noticeable after the particle passes  $x/\delta=16$ . Interestingly enough, the trajectories using HM2CH and HM4CH are nearly the same as that obtained by the spectral interpolation up to  $x/\delta=40$ . The discrepancies in the estimated trajectories are exaggerated in a  $yz$  plane view [Fig. 1(c)], because a  $yz$  plane view can provide the secondary flow patterns caused by turbulent structures near the wall. The trajectories begin to be contaminated in the near-wall region by numerical interpolation errors.

The sample time histories of the velocity and acceleration of a fluid particle that is released at the center of the channel are displayed in Fig. 2. The Lagrangian acceleration was calculated by using the second-order time-accurate difference scheme. Time history of the streamwise velocity is shown in Fig. 2(a) in which the estimated velocity using Linear shows a slight deviation from the exact one (Spectral) right after the particle tracking begins. The discrepancy be-

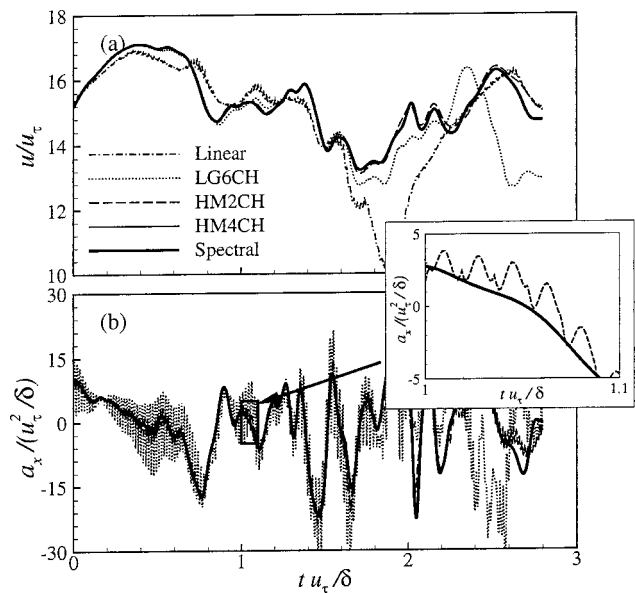


FIG. 2. Time histories of velocity and acceleration of a particle released at the center of channel using different interpolation schemes.

tween the estimated velocity using LG6CH and the exact one is clearly seen in Fig. 2 after  $t=1.5u_\tau/\delta$  from the released instant. However, the estimated velocities using HM2CH and HM4CH are in good agreement with the exact velocity in the present particle tracking. When acceleration is evaluated by using the velocity gradient in time, the errors between the estimated accelerations and the exact one can be intensified because abrupt changes of the velocity cause large interpolation error. Figure 2(b) shows the time histories of the streamwise component of acceleration using the different interpolation schemes. The history of acceleration obtained by the linear interpolation is not included in Fig. 2(b) because the estimated acceleration has incomparably too much error as expected from the behavior of the estimated velocity. Unexpected small-scale fluctuations of acceleration are found in the prediction by LG6CH. A closer inspection of the acceleration for a short time interval ( $1.0 \leq t u_\tau/\delta \leq 1.1$ ) in Fig. 2(b) discloses that the oscillatory pattern albeit small is also observed in the prediction by HM2CH. This may give rise to undesirable errors in Lagrangian statistics for the acceleration. If the acceleration is obtained from the velocity which was obtained from any interpolation scheme using data at a few nearby grid points, the numerical errors can be generated when a particle crosses a grid point. This is because using different sets of data to get velocity before and after the particle crosses a grid point can cause discontinuous derivative.<sup>8</sup> It is interesting to find that the acceleration by HM4CH is exactly the same as that by Spectral for a sufficiently long time period. This result suggests that HM4CH should be applied to evaluate the small-scale variation of acceleration with good accuracy.

To quantify the interpolation errors of the position, velocity, and acceleration of fluid particles, the root-mean-squared difference between the interpolated quantity and the exact one is defined as

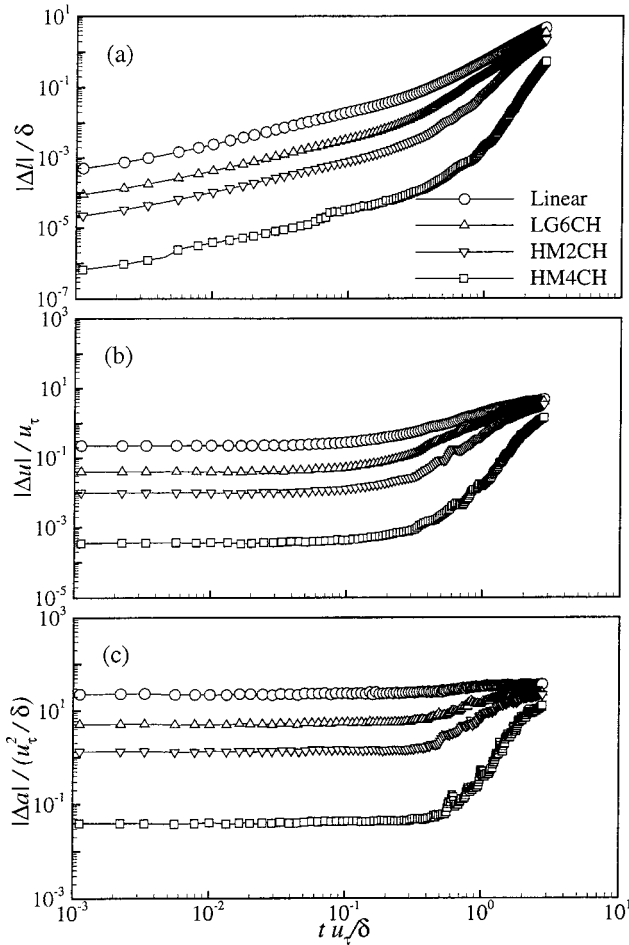


FIG. 3. Root-mean-squared errors for the position, velocity, and acceleration of 1024 particles using different interpolation schemes.

$$|\Delta\phi| = \sqrt{\frac{1}{N} \sum_{n=1}^N (\phi_i^n - \phi_e^n)^2}. \quad (4)$$

Here,  $\phi_i$  and  $\phi_e$  denote the interpolated and exact quantity, such as position, velocity and acceleration, and  $N$  is the number of particles. In the present study, 1024 particles are randomly released in the interior of the channel. Figure 3 shows the temporal growth of the errors as the fluid particles are tracked. The errors between the estimated position and the exact one are shown in Fig. 3(a). After the particles are released, the errors of the position are accumulated over time. The initial errors grow linearly with  $t$ , but the growth rate rapidly increases after  $tu_\tau/\delta \approx 0.3$  which is closely related with the Lagrangian integral time scale. It is natural that the smallest error can be obtained by using HM4CH. Figures 3(b) and 3(c) show the errors of the velocity and acceleration, respectively. Similarly, the smallest error is obtained when HM4CH is applied to the interpolation. The initial growth of the errors is nearly stationary in contrast to the position while the errors rapidly increase after the above characteristic time. It should be noted that the error caused by HM4CH is about two orders of magnitude smaller than that obtained by LG6CH.

TABLE I. Root-mean-squared position errors at  $2T_L$  and computational overhead.

	Linear	LG6CH	HM2CH	HM4CH	Spectral
$ \Delta l _{2T_L}/\delta$	0.458	0.186	0.042	0.001	...
CPU Time (sec.)	0.033	0.120	0.208	0.347	24.4

Although the highly accurate interpolation schemes and the time integration are applied to the particle tracking, the accumulative errors are inherent if the particle is numerically tracked during long time period. Therefore, it is important to know whether the errors of the Lagrangian quantities are allowable in the period to acquire the Lagrangian statistics. Root-mean-squared differences between the interpolated and the exact positions are summarized in Table I in terms of the interpolation errors at the twice Lagrangian integral time scales ( $T_L$ ). Table I shows that obviously the largest error appears in the linear interpolation scheme. It is interesting to see that the errors ( $|\Delta l|/\delta=0.001$ ) of HM4CH is smaller than the Kolmogorov length scale ( $\eta/\delta=0.03$ ) at the center of the channel. The CPU times on COMPAQ-DS20E required for the interpolation are also listed in Table I. Necessarily, higher-order interpolation schemes need more computational time. Conclusively, adopting HM4CH appears to produce most reliable Lagrangian statistics including acceleration statistics with a reasonable amount of computation overhead (Table I). Finally it is worthwhile to mention that an even higher-order or more accurate interpolation scheme is not necessary for meaningful Lagrangian statistics since by the time the interpolation error gets large enough, most Lagrangian quantities are decorrelated with the initial values.

#### IV. LAGRANGIAN STATISTICS

The Lagrangian trajectory of a single particle is not usually of major importance in a particle dispersion process. Detailed Lagrangian particle flow should be analyzed by the ensemble averaged quantities, such as the particle dispersion, correlation, Lagrangian structure function and so on. In the previous section, we have assessed the performance of the spatial interpolation schemes. Among the interpolation schemes, we adopt the HM4CH schemes for the particle tracking in all the following computations. Particle statistics were obtained for channel flow at  $Re_\tau=200$  and 400. To examine the inhomogeneity of Lagrangian statistics, a number of particles are released at the several wall-normal locations and then tracked. The Lagrangian statistics have been obtained by releasing 1024 particles from each of four different  $xz$  planes:  $y^+=5.22, 30.2, 100, 200$  for  $Re_\tau=200$  and  $y^+=5.34, 30.4, 99.3, 200$  for  $Re_\tau=400$ . These selections were made such that different behaviors were expected to be observed for particles released in the sublayer, buffer layer and log layer. For unbiased universal statistics, averaging was made not only over an ensemble of independent particle trajectories, but also over an ensemble of independent turbulence realizations.<sup>9</sup> In the present study, the independent 100 sets of particles were newly released every  $t^+=80$  which is sufficient to avoid a biased turbulence. Each particle was

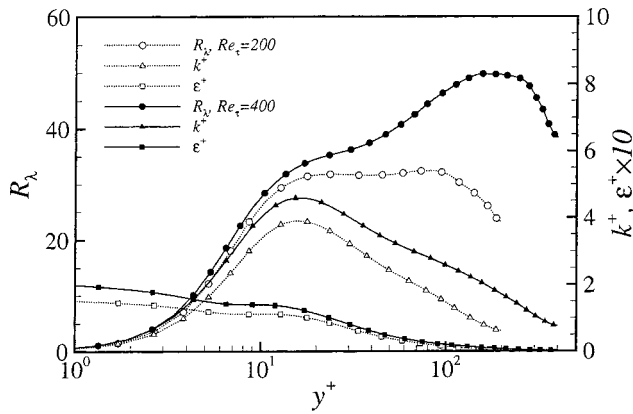


FIG. 4. Taylor-scale Reynolds number  $R_\lambda$ , kinetic energy  $k^+$  and dissipation rate  $\epsilon^+$  along the wall-normal direction.

tracked up to  $t^+ = 400$ , which is long enough for careful investigation of long-time variation. The Lagrangian integral time scale, typical decorrelation time of the velocity correlation, ranges from 4 to 100 wall units for the released positions given above, with the maximum occurring at  $y^+ = 200$  (see below). The tracking time steps are  $\Delta t_{tr}^+ \approx 0.08$  for both  $Re_\tau = 200$  and  $Re_\tau = 400$ , smaller than the smallest Kolmogorov time scale of order 1 wall unit, which guarantees negligible time-stepping errors compared with the suggestion in Kontomaris *et al.*<sup>9</sup>

Prior to the discussion on the Lagrangian statistics, we investigate the inhomogeneity of Eulerian flow quantities which are necessary for the analysis of the Lagrangian statistics. Figure 4 shows the turbulent kinetic energy ( $k^+$ ) and dissipation rate ( $\epsilon^+$ ) along the wall-normal direction. Since the flow is not isotropic, the Taylor-scale Reynolds number is defined as  $R_\lambda = \sqrt{(20/3)(k^+/\epsilon^+)}$  and the variation of  $R_\lambda$  in the wall-normal direction is shown in Fig. 4. In the vicinity of the wall,  $R_\lambda$  increases with the distance from the wall while  $R_\lambda$  decreases slightly near the center. Except for the above two limiting regions,  $R_\lambda$  is nearly constant around  $R_\lambda \sim 32$  for  $Re_\tau = 200$  and  $R_\lambda \sim 48$  for  $Re_\tau = 400$ . In the constant  $R_\lambda$  region, we can investigate the inhomogeneity of Lagrangian statistics excluding the influence of the Reynolds number. Later, the representative values of several Lagrangian quantities in this region will be compared to other simulation results.

**A. Velocity correlations**

For a statistically stationary flow, the velocity auto-correlation function  $\rho_{ii}(t)$  is defined as

$$\rho_{ii}(t) = \frac{\langle v_i(t_0)v_i(t+t_0) \rangle}{\langle v_i^2(t_0) \rangle^{1/2} \langle v_i^2(t+t_0) \rangle^{1/2}}, \tag{5}$$

where  $v_i$  is the turbulent fluctuation velocity of the Lagrangian particle and  $t_0$  is the released time and the auto-correlation does not depend on  $t_0$  due to stationarity. The subscript  $i$  denotes the direction of the velocity, i.e.,  $v_1$ ,  $v_2$ , and  $v_3$  are streamwise, wall-normal and spanwise velocity, respectively. The bracket  $\langle \rangle$  denotes the ensemble-averaged quantity. The repeated index does not imply summation here-

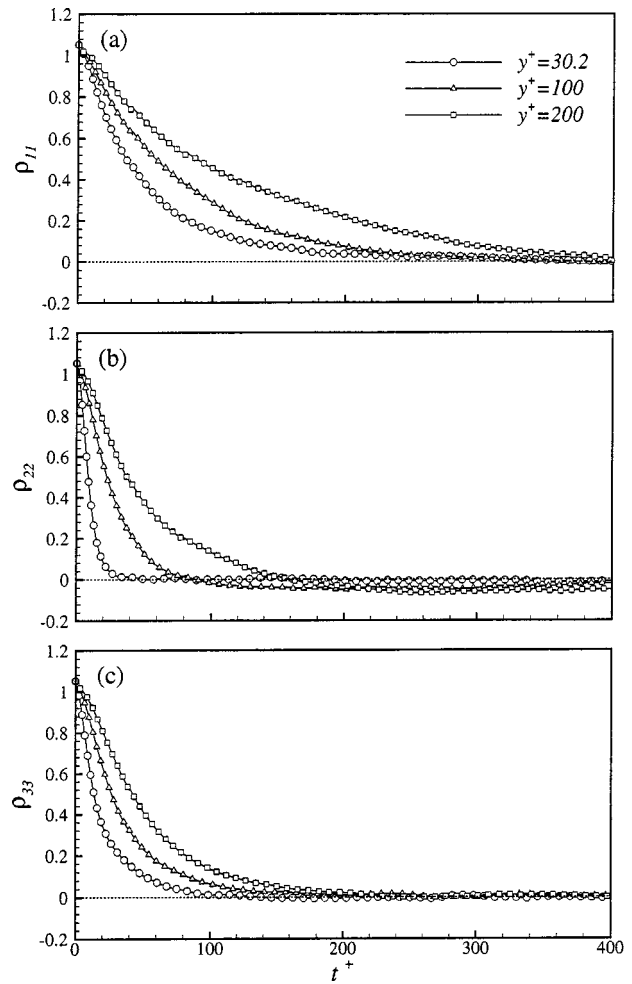


FIG. 5. Velocity auto-correlations of fluid particles released at the different wall-normal locations. (a) Streamwise, (b) wall-normal, and (c) spanwise velocity.

after. In the present channel flow, the streamwise velocity in Eulerian frame has a mean varying in the wall-normal direction due to the inhomogeneity from the existence of the wall. The Lagrangian fluctuation velocity  $v_i(t)$  is obtained from extracting the Eulerian mean velocity  $U_i[\mathbf{X}(t)]$  at the instantaneous particle position  $\mathbf{X}(t)$  from the Lagrangian particle velocity, as similarly applied in homogeneous turbulent shear flow.<sup>23</sup> It should be noted that  $\langle v_i^2(t+t_0) \rangle^{1/2}$  changes with time unlike homogeneous turbulence.

Figure 5 shows the effect of the released position of fluid particles on the Lagrangian velocity autocorrelation functions. The correlation functions are shown up to  $t^+ = 400$  for  $Re_\tau = 400$ , because the particle velocity is no more correlated with an initial velocity after  $t^+ = 400$ . As the initial particle position is located closer to the wall, the decaying rates of the correlation of all components are accelerated. Specially, both the wall-normal and spanwise velocities become decorrelated faster than the streamwise velocity. This is closely related with the presence of small-scale vortical structures near the wall such as the streamwise vortices. Investigation of the flow field near the wall clearly explains different correlation property between each component. Figure 6 shows two representative fluid particles released at  $y^+ = 13$  and the

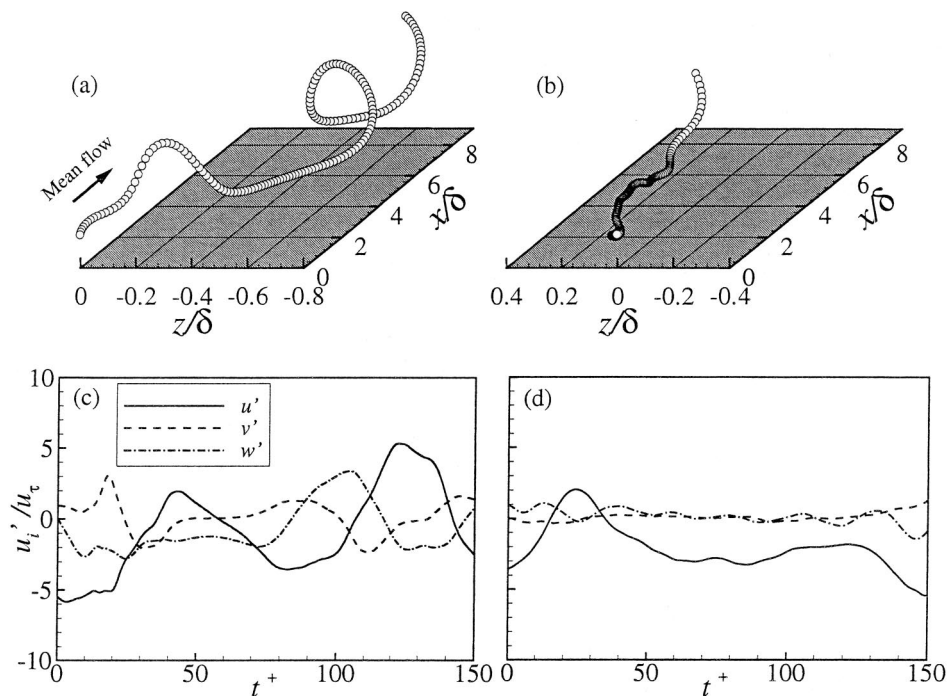


FIG. 6. Trajectories of two particles released at  $y^+ = 13$  and the corresponding temporal variation of the fluctuation velocity.

corresponding temporal variation of velocity components along the trajectories. Here, the mean Eulerian streamwise velocity is subtracted from the streamwise velocity. The helical trajectory of Fig. 6(a) is associated with a streamwise vortex, thus the wall-normal and spanwise velocities exhibiting an oscillatory pattern with the period of  $T^+ = 80$  as shown in Fig. 6(c). The other kind of trajectory in Fig. 6(b) is found in the low-speed streak, which is almost straight in the streamwise direction [note that different scales are used in the streamwise and spanwise directions in Figs. 6(a) and 6(b)], thus contributing almost nothing to the wall-normal and spanwise velocity correlations. Therefore, an ensemble average results in the rapidly decaying correlation near the wall as shown in Figs. 5(b) and 5(c). On the other hand, the streamwise velocity associated with the streamwise vortex obviously oscillates with the same period as the wall-normal or spanwise components as shown in Fig. 6(c), whereas the nonvanishing streamwise velocity in the low-speed streak exhibits a variation in much longer time scale as shown in Fig. 6(d). Summing all contributions yields a relatively slowly decaying correlation of Fig. 5(a). We investigate many other trajectories, finding similar behavior. Therefore, it can be concluded that the near-wall structure such as low-speed streaks are responsible for the different correlation characteristics between each velocity components. Armenio *et al.*,<sup>26</sup> however, observed in their LES of channel flow that the streamwise velocity correlates with itself for much longer time than our results for  $\rho_{11}$ . This is because they evaluated the correlation including the mean streamwise velocity component. The wall-normal component tends to decorrelate with itself faster than the other components and even shows negatively correlated behavior. This is probably due to the presence of the wall which plays a role as an obstacle to vertical motion. The effect of the wall is mainly manifested

in the wall-normal and spanwise correlation for the entire channel, whereas the streamwise correlation is hardly influenced by the wall except for the region very close to the wall. As the release point moves away from the wall, the correlations become more isotropic than the near-wall region.

As a quantitative measure of the time interval over which the particle velocity is correlated with itself, the Lagrangian integral time scale  $T_{Li}$  is defined in the present study as

$$T_{Li} = \int_0^{4T_{Ei}} \rho_{ii}(t) dt. \quad (6)$$

Although the Lagrangian integral time scales should be obtained by the integration of the correlation function on the time interval  $(0, \infty)$ , practically, the upper bound has to be finite. In the present study, the estimated Lagrangian time scale  $T_{Ei}$  is introduced and  $4T_{Ei}$  is used as the upper bound. Here,  $T_{Ei}$  is defined as twice the value of the time  $t$  at which the Lagrangian correlation coefficient is equal to  $e^{-1/2}$ . Variations of the Lagrangian integral time scales together with Kolmogorov time scales in the wall-normal direction are shown in Fig. 7(a). The Kolmogorov time scale monotonically increases with the distance from the wall. As expected, the Lagrangian time scales increase with the distance from the wall. It may be concerned with the inhomogeneity resulting from the presence of the wall. The Lagrangian time scale in the streamwise direction is longer than those in other directions in the whole region of the channel. Specially near the wall, the fluid particle velocity in the streamwise direction is correlated with itself for much longer time than in the other directions because of the turbulent structures near the wall as explained above. On the other hand, the Lagrangian

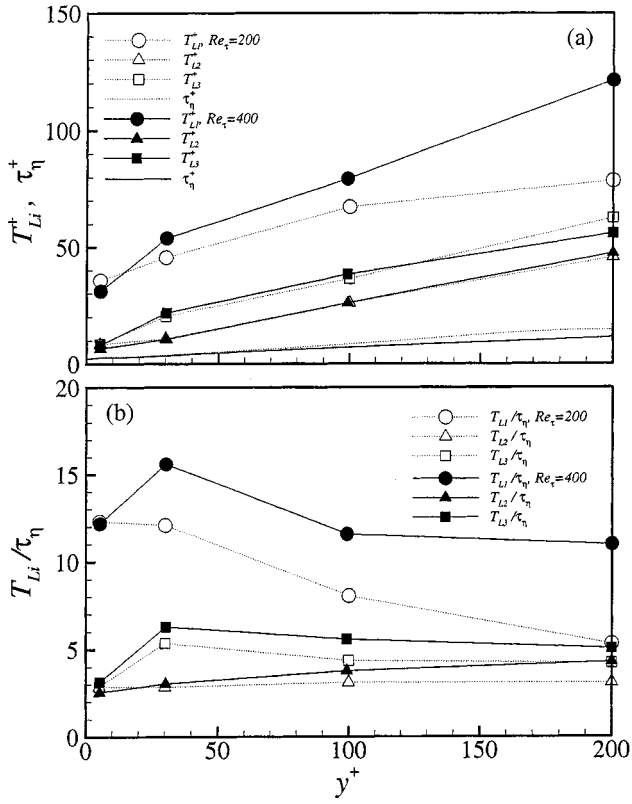


FIG. 7. Lagrangian integral time  $T_{Li}$  and Kolmogorov time scale  $\tau_\eta$  along the wall-normal direction.

time scales normalized by the Kolmogorov time,  $T_{Li}/\tau_\eta$ , exhibit an opposite trend in Fig. 7(b): As the initial position of the particle approaches the wall,  $T_{L1}/\tau_\eta$ , increases while  $T_{L2}/\tau_\eta$  and  $T_{L3}/\tau_\eta$  remain at almost the same level. This increase in level of anisotropy near the wall implies that a coherent structure has a preferred direction in location itself near the wall. Streamwise vortices and low-speed streaks are good examples that show such behavior. Figure 7 also shows dependence of  $T_{Li}$  on the Reynolds number. Particularly  $T_{L1}$  increases with the Reynolds number in more sensitive manner than  $T_{L2}$  and  $T_{L3}$ .

**B. Dispersion statistics**

Fluid particle dispersion is defined as the ensemble-averaged displacement of particles relative to the initial position.

$$\sigma_{X_i}^2(t) = \langle (X_i(t) - X_i(0))^2 \rangle. \tag{7}$$

An application of the classical Taylor's theory to homogeneous flow with uniform mean streamwise velocity  $U$  yields

$$\sigma_{X_i}^2(t) = (U^2 \delta_{i1} + \overline{u_i^2}) t^2, \quad t \ll T_{Li}, \tag{8}$$

$$\sigma_{X_i}^2(t) = U^2 \delta_{i1} t^2 + 2\overline{u_i^2} T_{Li} t, \quad t \gg T_{Li}, \tag{9}$$

where  $\overline{u_i^2}$  denotes turbulent intensity in the Eulerian frame for each direction. When  $U=0$ , Eqs. (8) and (9) reduce to classical scaling relations for each time range. Since the mean streamwise velocity in the channel flow is relatively

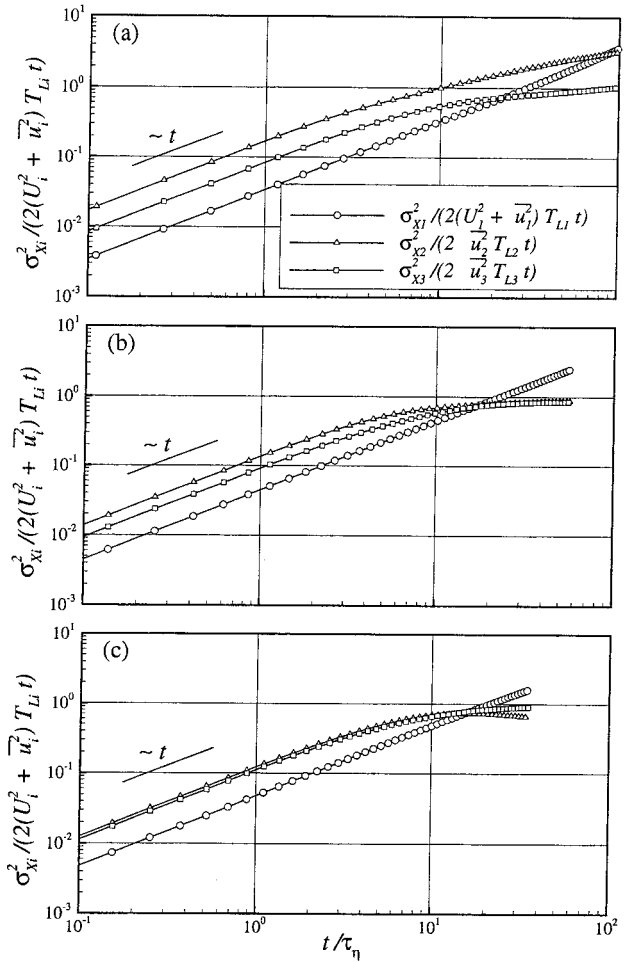


FIG. 8. Fluid particle dispersion in the inertial range for three release locations: (a)  $y^+ = 30.4$ ; (b)  $y^+ = 99.3$ ; (c)  $y^+ = 200$ .

uniform except for the region very close to the wall, the dispersion normalized by  $2(U^2 \delta_{i1} + \overline{u_i^2}) T_{Li} t$  for three different release locations are illustrated in Fig. 8. Here, the values of  $U$ ,  $\overline{u_i^2}$ , and  $T_{Li}$  at the release location are used. In most cases, the streamwise mean velocity is much greater than turbulence intensity, resulting in that the normalized dispersion in the streamwise direction grows linearly with time in the whole region as shown in Fig. 8. Quantitatively, the value of the normalized streamwise dispersion at  $t = \tau_\eta$  according to Eq. (8),  $0.5\tau_\eta/T_{L1}$ , is confirmed. When the mean shear is taken into account, the late-time dispersion is known to be cubically proportional to time,<sup>23,32</sup> i.e.,

$$\sigma_{X1}^2(t) = \frac{2}{3} S^2 \overline{u_2^2} T_{L2} t^3, \tag{10}$$

where  $S$  is the shear rate,  $dU_1/dx_2$ , which is assumed to be constant. Such a behavior of the streamwise dispersion is not observed in the region investigated for the two reasons that the mean shear is weak and that the wall-normal dispersion is bounded by the walls.

On the other hand, the horizontal dispersion at the early stage follows Eq. (8) very well as shown in Fig. 8. For the three release locations, this was confirmed quantitatively. According to Eq. (9), the normalized dispersion in late times should approach 1. Investigation of Fig. 8 reveals that in

most cases except the wall-normal dispersion of particles released at  $y^+ = 30.4$ , it is the case. Still, the normalized dispersion approaches a finite value greater than 1. This is because by the time particles disperse over more than one integral time, the particles do not have memory of the initial location any more, thus intensity and integral time scale being changed. Therefore, scaling by those values at the release point can overestimate dispersion. In summary, the effect of the mean shear is minimal and the classical Taylor dispersion is valid when the uniform mean flow is taken into account instead.

### C. Lagrangian structure function

In the Lagrangian frame, it is important to examine the behavior of the increment of velocity in time following a single fluid particle. The second moment of the increment is well known as the second-order Lagrangian structure function defined as

$$D_{ii}(t) = \langle (v_i(t+t_0) - v_i(t_0))^2 \rangle. \quad (11)$$

The application of classical Kolmogorov's similarity hypothesis to the Lagrangian structure function was given by Monin and Yaglom.<sup>2</sup> The initial asymptotic behavior according to the first Kolmogorov's hypothesis for sufficiently high Reynolds number is

$$D_{ii}(t) = a_0 \langle \epsilon \rangle^{3/2} \nu^{-1/2} t^2, \quad t \ll \tau_\eta, \quad (12)$$

where  $\langle \epsilon \rangle$  is the averaged dissipation rate and  $a_0$  is assumed to be universal constant which is approximately 1 in a model assuming Gaussian fluctuations.<sup>7,14</sup> The Lagrangian structure functions in small-scale range are investigated to reveal the quadratic dependence on time for small  $t/\tau_\eta$  in accord with Eq. (12). For more detailed variation of  $a_0$ , the acceleration variances can be investigated since Eq. (12) simply means  $a_0 = \overline{a_i^2} / (\langle \epsilon \rangle^{3/2} \nu^{-1/2})$  where  $\overline{a_i^2}$  denotes mean-square acceleration. This approach has an advantage that the acceleration can be obtained in the Eulerian frame by calculating the right hand side of Eq. (1) and, therefore, particle tracking is not necessary, thus interpolation and differentiation errors not occurring. It was confirmed that both calculations yield the same  $a_i$ .

Kolmogorov's first hypothesis implies that in isotropic turbulence the variance of acceleration is universal when the acceleration is scaled by the local dissipation rate and viscosity. It has been reported that at low Reynolds number flow, Kolmogorov constant  $a_0$  is not universal and depends on  $R_\lambda^{1/2}$  in stationary isotropic turbulence.<sup>8</sup> Similar trend was observed in the recent experiments.<sup>7,14</sup> In the present channel flow, this constant depends further on the initial particle position and direction of velocity. Corresponding  $a_0$  along the wall-normal direction is displayed in Fig. 9, clearly showing strong inhomogeneity but weak anisotropy in turbulent channel flow.  $a_0$  in all directions monotonically increases as the releasing position moves away from the wall except for the spanwise component at  $y^+ = 200$  for  $Re_\tau = 200$ , which is believed to be due to the symmetric property at the channel center. Despite high level of anisotropy of the velocity auto-

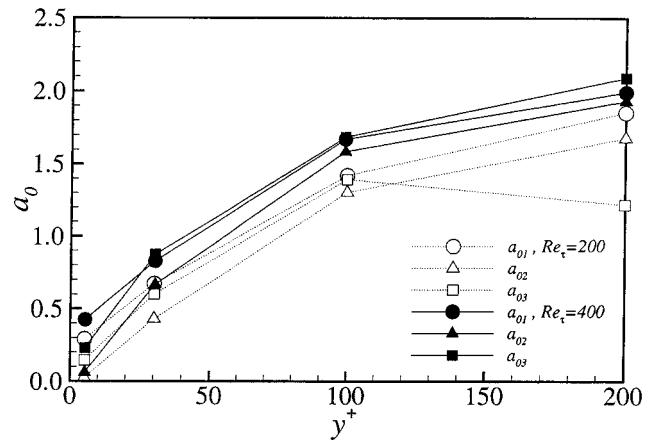


FIG. 9. Kolmogorov constant  $a_0$  in each direction along the wall-normal direction.

correlation near the wall,  $a_0$  does not exhibit such anisotropic behavior, probably due to the fact that acceleration is dominantly determined by structures of small length and time scales. The acceleration of a fluid particle in turbulent flow arises from the viscous damping and the pressure gradient term, where the viscous damping term is small compared to the pressure gradient term in homogeneous flow.<sup>7,13</sup> In the channel flow, however, viscous damping term in the streamwise direction is not negligible specially very near the wall, which is responsible for the nontrivial value of  $a_0$  in the streamwise direction near the wall in Fig. 9. Thus, the directional variance of  $a_0$  tends to be localized to the viscous sublayer. With the increase of the Reynolds number,  $a_0$  increases slightly for all components for the same release position in wall unit.

Kolmogorov's second hypothesis suggests the behavior of the Lagrangian structure function in the inertial range as

$$D_{ii}(t) = C_0 \langle \epsilon \rangle t, \quad \tau_\eta \ll t \ll T_{Li}. \quad (13)$$

Kolmogorov constant  $C_0$  is an essential parameter because it implies the rate of de-correlation of Lagrangian velocity fluctuations, similar to the Kolmogorov constant in the Eulerian structure function  $C_0^E (\equiv \langle (u_i(x+r) - u_i(x))^2 \rangle / (\langle \epsilon \rangle^{2/3} r^{2/3})$ ). The value of  $C_0^E$  is relatively well known to be approximately 2 in the longitudinal direction of the channel<sup>33</sup> and linked directly to Kolmogorov constants in one- and three-dimensional energy spectrum in wave number space.<sup>34</sup> In contrast to  $C_0^E$ ,  $C_0$  is rather uncertain<sup>35</sup> and has been widely investigated within the scope of homogeneous turbulence. To investigate  $C_0$ , the scaled Lagrangian structure function  $D_{ii} / (\langle \epsilon \rangle t)$  is plotted against  $t/\tau_\eta$  in Fig. 10. A plateau of  $C_0$  within the inertial range should be observed according to the Kolmogorov similarity. In practice, however, for a low Reynolds number isotropic turbulence Yeung and Pope<sup>4</sup> found that such plateaus of  $C_0$  are not observed, instead the local maximum value  $C_0^*$  appears in the Lagrangian structure function, of which the value increases with  $R_\lambda$ . In the present study, the plateaus of  $C_0$  are not observed and  $C_0^*$  depends on the initial particle locations and directions as

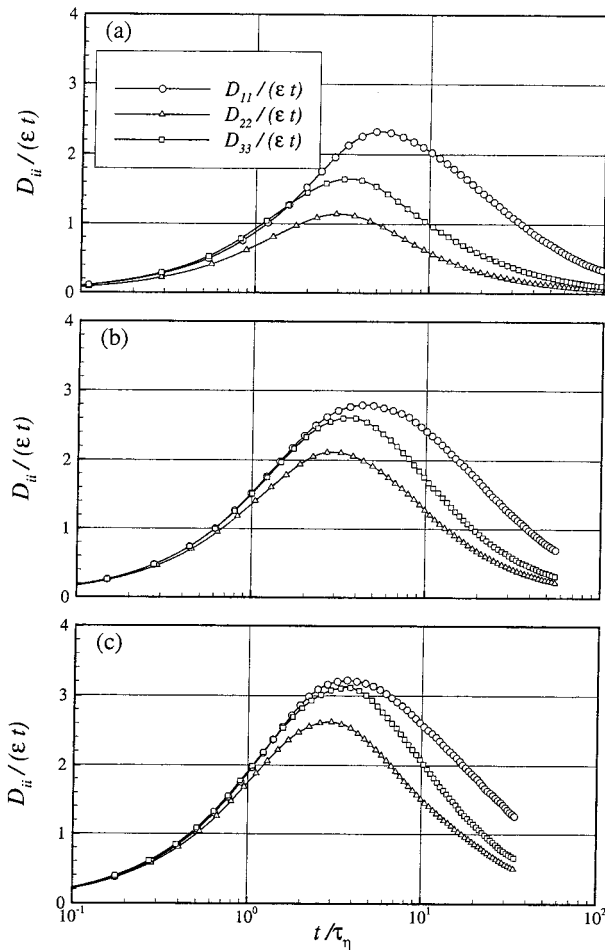


FIG. 10. Scaled Lagrangian structure functions in the inertial range for three release locations: (a)  $y^+ = 30.4$ ; (b)  $y^+ = 99.3$ ; (c)  $y^+ = 200$ .

well. Wherever the particles are released,  $C_0^*$  for the streamwise direction is larger than for the other directions. Although  $C_0^*$  in the isotropic turbulence is reportedly located at about  $t = 4.5\tau_\eta$  for all Reynolds numbers,<sup>4</sup> the local maximum instants are found in  $2.5\tau_\eta \leq t \leq 5\tau_\eta$  depending on the initial location and direction.

To investigate the effect of the inhomogeneity and anisotropy,  $C_0^*$  is displayed against the initial particle position in Fig. 11. Typical reported values of  $C_0^*$  range from 2.5 to 4.5 for  $R_\lambda$  between 38 and 240 in the isotropic turbulence.<sup>35</sup> As shown in Fig. 4,  $R_\lambda$  ranges from 25 to 32 for  $Re_\tau = 200$  and from 36 to 49 for  $Re_\tau = 400$  except for the near wall region  $y^+ \leq 15$  in the present channel flow. The corresponding  $C_0^*$  ranges from 0.5 to 3.0. In the streamwise direction,  $C_0^*$  is approximately  $2.5 \pm 0.5$  for  $Re_\tau = 400$ , which is consistent with the previous founding for isotropic turbulence  $Re_\lambda = 38$  considering Reynolds number dependence.<sup>4</sup> Unlike the normalized acceleration variance  $a_0$  in Fig. 9,  $C_0^*$  in the streamwise direction is larger than those in other directions and nearly constant when the initial particle location is sufficiently far from the wall. However,  $C_0^*$  in the spanwise direction increases as the releasing position moves away from the wall and further increases for  $Re_\tau = 400$  while it decreases towards the center of channel for  $Re_\tau = 200$ , which

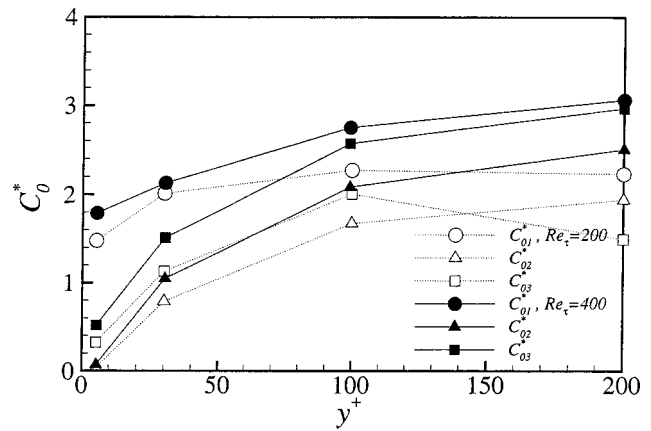


FIG. 11. Local maximum of the scaled Lagrangian structure function  $C_0^*$  in each direction along the wall-normal direction.

is believed to be the effect of the center. On the other hand,  $C_0^*$  in the wall normal direction monotonically increases with the distance far from the wall. This inhomogeneity may be attributed to the nontrivial variations of the energy dissipation rate along the path traced out by some fluid particle over time.<sup>8</sup> Overall,  $C_0^*$  in each direction approaches each other with the distance from the wall while it shows significant anisotropy near the wall. For all release points,  $C_0^*$  increases as the Reynolds number increases.

Since our dispersion simulations were carried out for two very low Reynolds number flows, it is very difficult to investigate the dependence of the statistics on the Reynolds number. However, for comparison purposes,  $T_L/\tau_\eta$ ,  $a_0$  and  $C_0^*$  for the representative  $R_\lambda$  are shown with the reported values for isotropic flow in Fig. 12. Here, the representative values of each quantity were obtained by averaging two values at  $y^+ \approx 30$  and  $y^+ \approx 100$  for  $Re_\tau = 200$  and by adopting the value at  $y^+ = 200$  for  $Re_\tau = 400$  in Figs. 7, 9, and 11, since  $R_\lambda$  is quite uniform in the region, as shown in Fig. 4. For  $T_L/\tau_\eta$  [Fig. 12(a)], the relation proposed by Sawford,<sup>15</sup>  $T_L/\tau_\eta = 2R_\lambda/C_0 15^{1/2} (1 + 7.5C_0^2 R_\lambda^{-1.64})$  with  $C_0 = 6$ , which was obtained by second-order Lagrangian stochastic theory, is drawn together. As expected, high level of anisotropy in  $T_L$  is observed between the streamwise and other directions. However, the dependence on the Reynolds number is not confirmed. For  $a_0$ , the power-law relation,  $a_0 = 0.13R_\lambda^{0.64}$ , proposed by Sawford<sup>15</sup> is drawn together. Although the Reynolds numbers are quite low, strong isotropy is observed, which is favorable from the stochastic modeling point of view. Since  $a_0$  is a local quantity scaled by viscosity, strong dependence on the Reynolds number is easily noticeable, suggesting a different scaling dependence on the Reynolds number. Similarly, the representative value of  $C_0^*$  is shown in Fig. 12(c). Lines drawn are the correlation obtained by a Lagrangian stochastic model.<sup>35</sup> Compared to the shear flow cases, similar kind of anisotropy is observed for  $R_\lambda = 48$  in that the wall-normal dispersion is most suppressed while the streamwise and spanwise dispersions are most enhanced. For  $R_\lambda = 32$ , however, the spanwise dispersion is also suppressed.

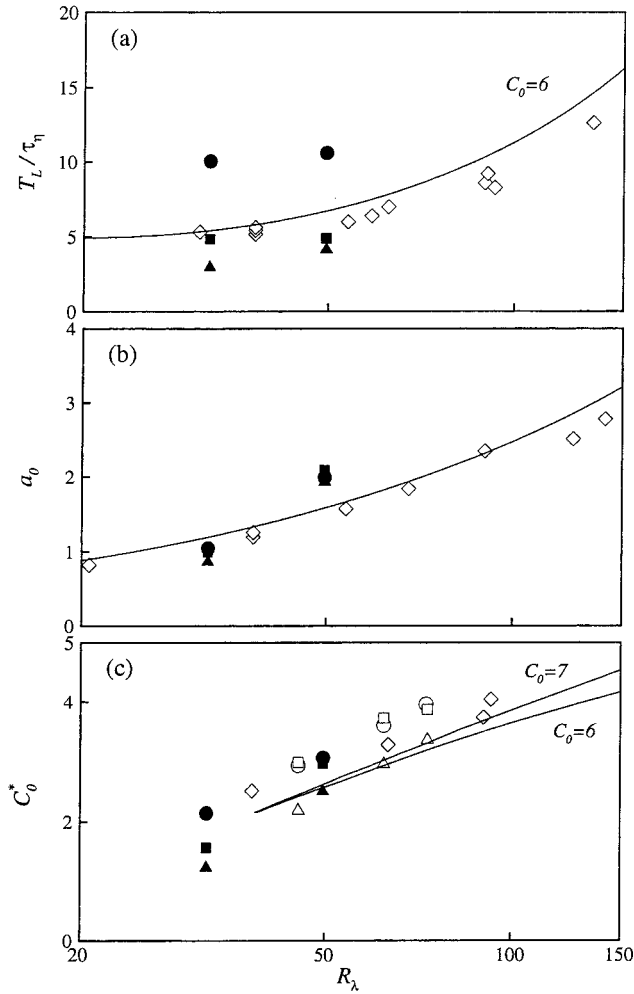


FIG. 12. Reynolds number dependence of (a) Lagrangian time scale  $T_L/\tau_\eta$ , (b) Kolmogorov constants  $a_0$ , and (c) local maximum of the scaled Lagrangian structure function  $C_0^*$  in the streamwise ( $\bullet$ ), wall-normal ( $\blacktriangle$ ), and spanwise ( $\blacksquare$ ) directions for the present simulation and for isotropic turbulence (Ref. 4) ( $\diamond$ ). The lines are from stochastic model (Refs. 15 and 35) using the indicated values of  $C_0$ . The open symbols ( $\circ, \triangle, \square$ ) represent the corresponding values for the homogeneous shear flow in the streamwise, wall-normal, and spanwise directions, respectively (Ref. 35).

#### D. Acceleration statistics

In this section, we investigate the Lagrangian statistics of the fluid particle acceleration in the turbulent channel flow. Recently, Lagrangian statistics of the fluid particle acceleration have been studied by direct numerical simulations of isotropic turbulence and homogeneous shear flow.<sup>23</sup> The previous finding is that the one-particle acceleration auto-correlation decays rapidly with time, with a zero crossing just over two Kolmogorov time scales.<sup>4,23</sup> In the present study, the one-particle acceleration correlation is evaluated in order to investigate the inhomogeneity due to the presence of the wall. Lagrangian particle acceleration is calculated by using a second-order accurate time derivative of the particle velocity. Similar to the Lagrangian velocity auto-correlations, the acceleration correlation is defined as

$$\rho_{ii}^a(t) = \frac{\langle a_i(t_0)a_i(t+t_0) \rangle}{\langle a_i^2(t_0) \rangle^{1/2} \langle a_i^2(t+t_0) \rangle^{1/2}}, \quad (14)$$

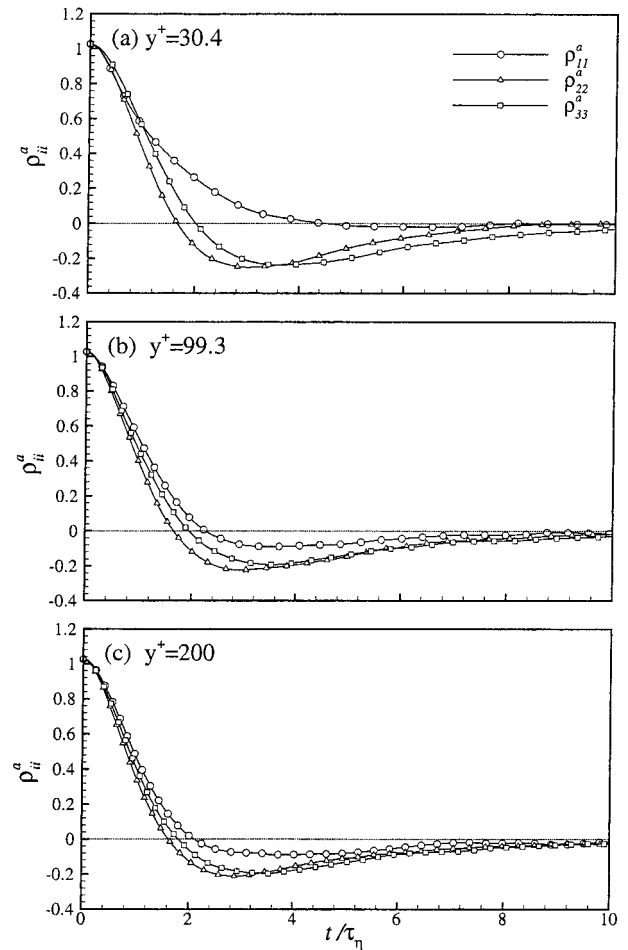


FIG. 13. Acceleration auto-correlations of fluid particles released at the different wall-normal locations against time normalized by the Kolmogorov time scale. (a)  $y^+ = 30.4$ , (b)  $y^+ = 99.3$ , and (c)  $y^+ = 200$ .

where  $a_i$  is particle acceleration and subscript  $i$  denotes the direction of acceleration.

Figure 13 shows the acceleration auto-correlation for three initial positions of particles against time normalized by the Kolmogorov time scale defined at the release location. Each acceleration is found to have essentially zero integral time scale because the negatively correlated part almost cancels the positive region. This is consistent with the results of the homogeneous shear flow.<sup>5</sup> Therefore, the zero crossing time scale was suggested as a characteristic time scale.<sup>5</sup> It is interesting to see that the zero-crossing time scale is estimated as about  $2\tau_\eta$  in all cases except for the correlation of the streamwise acceleration of particles released very near the wall. Considering the distribution of the Kolmogorov time scale (see Fig. 4), the decaying rate of the acceleration correlation decreases as the particle is released further away from the wall. This phenomenon is closely related with the fact that small-scale structures near the wall possess short-time scales. Investigation of acceleration field near the wall reveals that very localized wall-normal and spanwise accelerations of large amplitude are mainly associated with the near-wall streamwise vortices which are almost parallel with

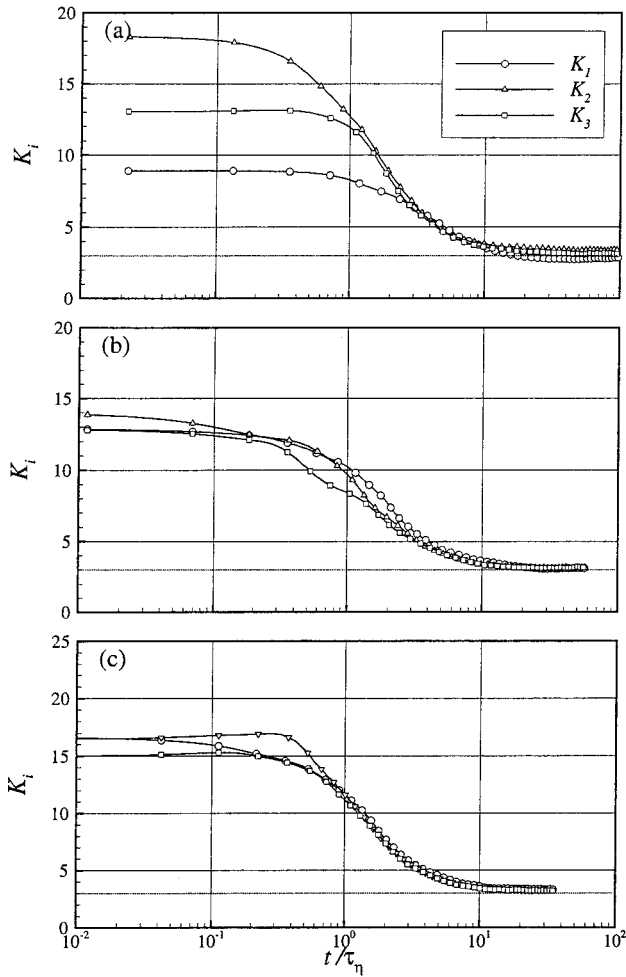


FIG. 14. Kurtosis of Lagrangian velocity structure function for three release locations: (a)  $y^+ = 30.4$ ; (b)  $y^+ = 99.3$ ; (c)  $y^+ = 200$ .

the wall, while the nonvanishing streamwise acceleration is found near the head of the streamwise vortices or the horse-shoe vortices. This suggests that the characteristic time scale associated with the streamwise acceleration is larger than those of the wall-normal and spanwise acceleration since the head of the streamwise vortices or the horse-shoe vortices are typically found a little farther away from the wall than the near-wall streamwise vortices. This explains that the streamwise acceleration correlates with itself for longer time than the other components as shown in Fig. 13(a).

As a measure of Gaussianity, the kurtosis of the Lagrangian structure function defined as

$$K_i(t) = \frac{\langle (v_i(t+t_0) - v_i(t_0))^4 \rangle}{\langle (v_i(t+t_0) - v_i(t_0))^2 \rangle^2}, \quad (15)$$

is investigated. In homogeneous turbulence, the accelerations exhibit highly intermittent behaviors.<sup>4,6,7,14</sup> It has been known that the accelerations many times the rms value are frequent in the probability density function of the acceleration.<sup>7</sup> Now, the effect of the inhomogeneity and anisotropy on the kurtosis  $K$  is examined in Fig. 14. When the particles are released, the flatness of Lagrangian structure function shows very high kurtosis level initially, which is

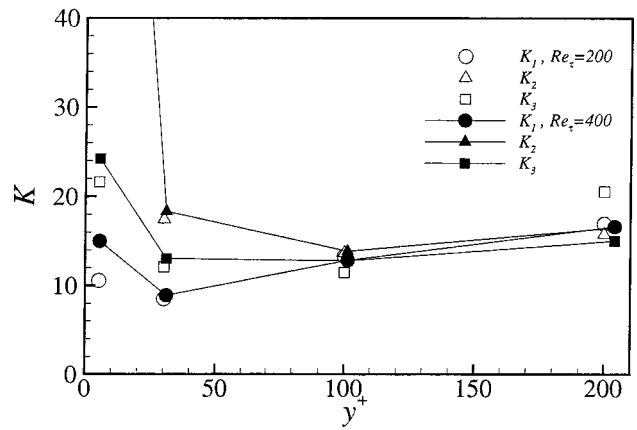


FIG. 15. Kurtosis  $K(0)$  along the wall-normal direction.

linked to high intermittency of acceleration. However, all of the kurtosis indicate that the distribution is expected to approach  $K \approx 3$ , typical value for the Gaussian shape after the particles are tracked for more than several Kolmogorov time scales, which is of order of the integral time scale of the velocity auto-correlation.

For very small time lag, the kurtosis of Lagrangian structure function approaches that of the acceleration component.<sup>4</sup> The initial kurtosis level of velocity increment along the wall-normal direction is displayed in Fig. 15 to disclose the effect of the particle position on the high kurtosis levels. Except for the near-wall region, the values of the kurtosis range from 10 to 20, which are consistent with that in isotropic turbulence.<sup>4</sup>  $K$  shows constant behavior at  $y^+ > 100$ , where the value is approximately 15. In the near-wall region, however,  $K$  shows the highly intermittent behavior specially in the wall-normal direction. In Fig. 15, the data of  $K = 131$  for  $Re_\tau = 200$  and  $K = 111$  for  $Re_\tau = 400$  in the wall-normal direction for the particles released at near wall region are not shown. This kind of high intermittency has never been observed. A close examination of a flow field in that region reveals that the wall-normal motion induced by the near-wall structures is greatly suppressed by the wall, specially the motion toward the wall, causing very large positive wall-normal acceleration. Figure 15 also suggests that the kurtosis is not a sensitive function of the Reynolds number. This is opposite to the experimental finding of La Porta *et al.*<sup>7</sup> that the Kurtosis rapidly increases with the Reynolds number at low Reynolds numbers although their Reynolds number is still high compared to ours. If the intermittent behavior of near-wall acceleration is linked with the near-wall coherent structures, such a universal trend of the kurtosis might be expected. However, it is not conclusive at this stage and further investigation is necessary.

### E. Probability density function of particle position

The study of Lagrangian statistics are extended to the probability density function (PDF) of the expected position of the drifting particles for  $Re_\tau = 200$ . To investigate the spatial distribution of the particles, two-dimensional PDF  $P(y, z; x)$  of the particle position is calculated by using the

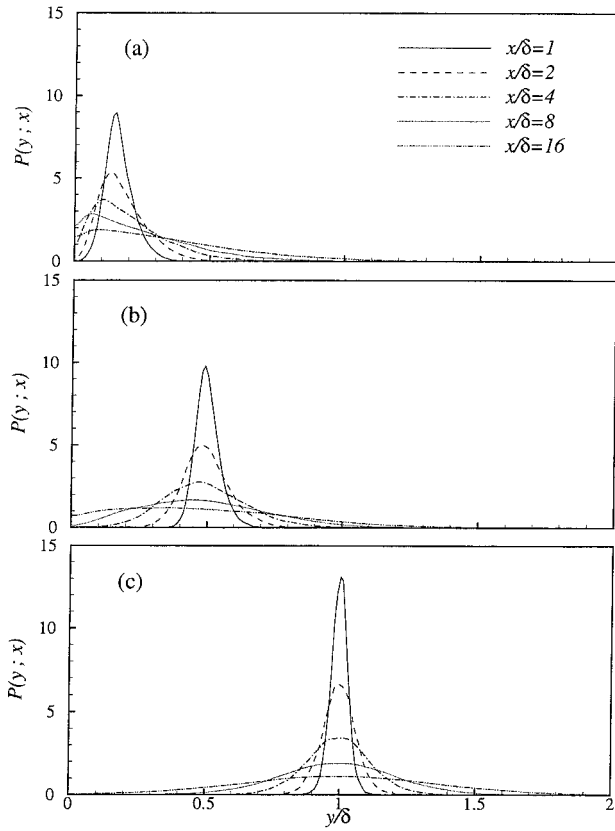


FIG. 16. Probability density function  $P(y;x)$  of expected wall-normal location of particles released at (a)  $y^+ = 30.2$ , (b)  $y^+ = 100$ , and (c)  $y^+ = 200$ .

Gaussian kernel regression<sup>36</sup> at several downstream locations. The mirror image of the weight function is used for impermeability in the near-wall region. The selected downstream locations are  $x/\delta = 1, 2, 4, 8,$  and  $16$  where the particles are released at  $x = 0$ . To obtain a quasi-steady distribution, particles are newly released at the particular wall-normal location after ninety percent of particles have passed through the final downstream location. The initial particle positions in the wall-normal direction are selected as  $y^+ = 30.2, 100,$  and  $200$ . Figure 16 shows the one-dimensional PDF  $P(y;x)$  along the wall-normal direction, which is obtained by integrating  $P(y,z;x)$  in the spanwise direction. As shown in Fig. 16, PDFs are fairly symmetrical at  $x/\delta = 1$ , but become more spread toward the wall with increasing  $x/\delta$ .<sup>27,28</sup> This asymmetric patterns are more augmented as the initial position is closer to the wall. Particles approaching to the near-wall region move shorter distance to the downstream. Consequently, the maximum PDF moves closer to the wall. However, PDF at the center has maintained a symmetric behavior. At sufficiently far downstream, the particles would be uniformly spread over the wall-normal direction. It is interesting to note that at the initial stage, the wall-normal dispersion is more active near the wall than at the center.

To quantify the spatial PDF in detail, the first and second moments of the PDF in the wall-normal and spanwise directions are defined as

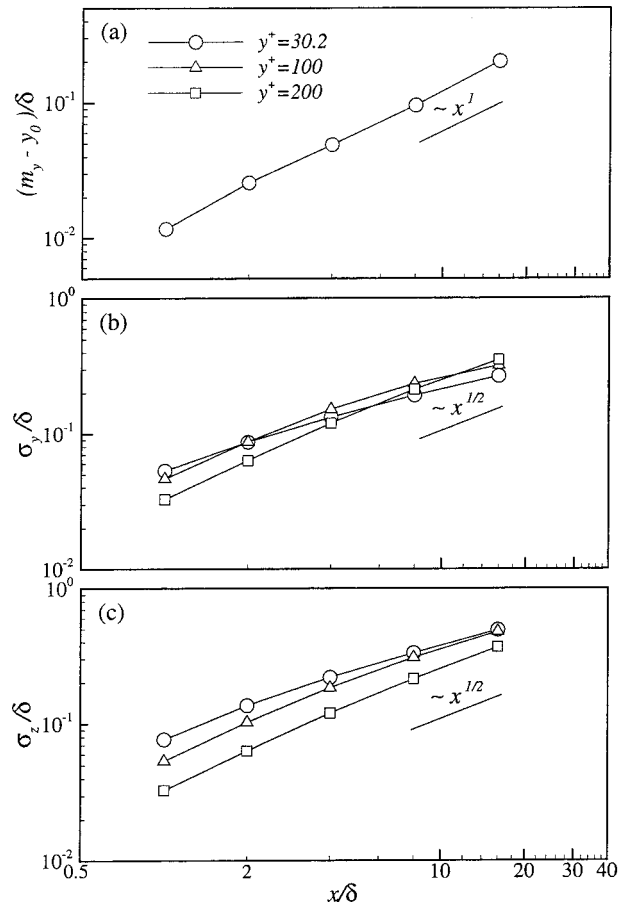


FIG. 17. Moments of probability density function  $P(y,z;x)$  of wall-normal particle location: (a) Mean position,  $(m_y - y_0)/\delta$ ; (b) spreading rate in the wall-normal direction,  $\sigma_y/\delta$ ; (c)  $\sigma_z/\delta$ .

$$m_y = \int \int y P(y,z;x) dy dz, \tag{16}$$

$$\sigma_y = \int \int (y - m_y)^2 P(y,z;x) dy dz, \tag{17}$$

$$\sigma_z = \int \int y^2 P(y,z;x) dy dz, \tag{18}$$

where  $m_y$ ,  $\sigma_y$ , and  $\sigma_z$  are the mean position and spreading rates in each direction, respectively. By symmetry the mean position in the spanwise direction is 0. The relative mean position  $(m_y - y_0)/\delta$  with the initial wall-normal particle location  $y_0$  is shown in Fig. 17(a). Here, the mean position for the particles released at  $y^+ = 100, 200$  are not shown since they remain almost zero for the region investigated. As the particles are released closer to the wall,  $(m_y - y_0)/\delta$  is more deviated with the increasing  $x/\delta$ , although the maximum PDF moves closer to the wall. The increment of  $(m_y - y_0)/\delta$  is directly linked with the long-tail of  $P(y;x)$  toward the center of channel, meaning biased dispersion due to the wall. The late-time behavior of the mean position grows linearly with the distance, i.e.,  $(m_y - y_0)/\delta \sim x$  as shown in Fig. 17(a). The spreading rates of PDFs to the wall-normal direction are also shown in Fig. 17(b). General trends are such that the particles spread more widely and rapidly at the downstream as the releasing position is further from the wall.

The spreading rate for the particle released at  $y^+ = 200$  shows a typical behavior of dispersion,  $\sigma_y \sim x^{1/2}$  while the dispersion of particles released near the wall behaves like  $\sigma_y \sim x^\alpha$  with  $\alpha < 1/2$ . Similarly, the moments of PDFs in spanwise direction are illustrated in Fig. 17(c). The spreading rates  $\sigma_z/\delta$  seems to approach  $x^{1/2}$  behavior unlike the wall-normal dispersion, meaning that the presence of the wall does not significantly influence the dispersion in the spanwise direction.

## V. CONCLUSIONS

Detailed numerical analysis has been performed to characterize the Lagrangian behavior of fluid particle in turbulent channel flow. Direct numerical simulations of turbulent channel flow at  $Re_\tau = 112, 200, \text{ and } 400$  were carried out in a spectral domain. The performance of the particle tracking algorithms were re-evaluated through comparison of errors in computed particle kinematic information against those obtained by spectral interpolation scheme for  $Re_\tau = 112$ . Root-mean-squared error of the particle position at the twice Lagrangian integral time scales shows that the error in HM4CH is smaller than the Kolmogorov length scale at the center of the channel. The oscillatory patterns in the estimated acceleration are observed for all interpolation schemes except for HM4CH. Adopting HM4CH appears to produce most reliable Lagrangian statistics including acceleration correlations with a reasonable amount of computational overhead.

To investigate the inhomogeneity of Lagrangian statistics, a large number of particles are released at the several wall-normal locations and then tracked using HM4CH for spatial interpolation scheme and the third-order Runge–Kutta scheme for time integration. Particle statistics have been calculated for the two cases of channel flow at  $Re_\tau = 200$  and  $400$ . Except for the near wall region, the present  $R_\lambda$  is observed to be nearly constant around  $R_\lambda \sim 32$  for  $Re_\tau = 200$  and  $R_\lambda \sim 48$  for  $Re_\tau = 400$ , respectively. The Lagrangian velocity auto-correlations are maintained for a long time in the order of streamwise, spanwise, and wall-normal direction, which is related with the elongated coherent structures near the wall. The initial dispersions indicate that the asymptotic behavior in the small-scale range would not depend on the initial position and direction. Contrast to the homogeneous turbulence, the initial dispersion should be normalized considering the mean streamwise velocity. The different asymptotic behavior of the dispersion in inertial range is related with the suppressed dispersion near the wall.

The normalized Lagrangian structure functions in small-scale and inertial ranges were investigated for the effect of inhomogeneity and anisotropy on Kolmogorov constants  $a_0$  and  $C_0$ . The scaled acceleration variance  $a_0$  in all directions increases with the distance from the wall with weak anisotropic property. The plateaus of  $C_0$  in the inertial range are not observed and instead the local maximum  $C_0^*$  depend on the initial particle location and direction. Unlike the behavior of the acceleration variance,  $C_0^*$  for the streamwise direction is larger than that for the other directions. The corresponding

$C_0^*$  ranges between 0.5 and 3.0. In the streamwise direction,  $C_0^*$  is approximately  $2.5 \pm 0.5$ , which is consistent with the results of low Reynolds number isotropic turbulence at  $R_\lambda = 38$ .  $C_0^*$  for the spanwise and wall-normal directions increases with the distance of the releasing position from the wall. The anisotropic behavior of  $C_0^*$  is more magnified when the initial particle position is closer to the wall. When the Kolmogorov constants were compared with the previous findings, the constants for the spanwise direction is closest to the isotropic relation, whereas high level of anisotropy is realized in the streamwise and wall-normal directions. The wall-normal dispersion is most suppressed while the streamwise dispersion is most enhanced. Although our simulations were carried out for two relatively low Reynolds numbers, dependence of  $T_L$ ,  $a_0$ , and  $C_0^*$  on the Reynolds number was investigated. Most quantities increase with the Reynolds number with different scaling relations as shown in Fig. 12.

The inhomogeneity of the acceleration correlation for the initial position of particles was also examined. The acceleration is rapidly de-correlated as the particle is released further away from the wall. Accelerations are found to have essentially zero integral time scales. The zero-crossing time scale is estimated to be about  $2\tau_\eta$ , which is similar to that in homogeneous turbulence except for the streamwise acceleration. The characteristic time scale for the streamwise acceleration is larger than those of the wall-normal and spanwise acceleration due to the near-wall streamwise vortices. The effect of the inhomogeneity and anisotropy on the kurtosis  $K$  of Lagrangian structure function was also examined. For very small time lags,  $K$  in the near wall region shows the highly intermittent behavior specially in the wall-normal component of acceleration.

Finally, the spatial probability density functions (PDF) of the position of the drifting particles were investigated. Asymmetric patterns of the spatial PDFs are magnified as the initial position is close to the wall. The mean of particle position in the wall-normal direction deviates from the initial position as the particles move downstream, while the maximum PDF moves closer to the wall. The increment of mean position is directly linked with the long-tail of PDFs toward the center of channel. However, the dispersion in the spanwise direction is homogeneous and the spreading rates increases with downstream.

## ACKNOWLEDGMENT

This research was supported by a grant from KOSEF (R01-2000-000-00306-0).

## APPENDIX: HERMITE–CHEBYSHEV INTERPOLATION

The fourth-order Hermite interpolation<sup>11</sup> is expanded to two dimensions for the homogeneous directions, such as  $x$  and  $z$  directions and combined with Chebyshev interpolation in the wall-normal direction. The scheme is specified as

$$\begin{aligned} \mathbf{V}(\mathbf{X}, t) = & \sum_{l=1}^N \sum_{m=1}^N \sum_{n=0}^{N_y} [\hat{\mathbf{U}}(l, n, m, t) H_l(x) H_m(z) \\ & + \hat{\mathbf{U}}_x(l, n, m, t) G_l(x) H_m(z) \\ & + \hat{\mathbf{U}}_z(l, n, m, t) H_l(x) G_m(z) \\ & + \hat{\mathbf{U}}_{xz}(l, n, m, t) G_l(x) G_m(z)] T_n\left(\frac{y}{\delta}\right). \end{aligned} \quad (\text{A1})$$

Here,  $\hat{\mathbf{U}}$ ,  $\hat{\mathbf{U}}_x$ ,  $\hat{\mathbf{U}}_z$ , and  $\hat{\mathbf{U}}_{xz}$  are Fourier–Chebyshev coefficients for the Eulerian velocity and its derivatives.  $N=2$  corresponds to the classical two-point Hermite interpolation scheme. When the interpolation point  $(x, z)$  is located in between  $(x_i, z_k)$  and  $(x_{i+1}, z_{k+1})$ . The basis functions for the two-point Hermite interpolation can be written as

$$\begin{aligned} H_1(\xi) &= 2\xi^3 - 3\xi^2 + 1, \\ H_2(\xi) &= -2\xi^3 + 3\xi^2, \\ G_1(\xi) &= (\xi^3 - 2\xi^2 + \xi)h, \\ G_2(\xi) &= (\xi^3 - \xi^2)h, \end{aligned} \quad (\text{A2})$$

where  $\xi = (x - x_i)/h$  or  $\xi = (z - z_k)/h$  and  $h$  is the grid spacing.

When the Hermite interpolation is applied, the exact information for the velocity derivatives is required in order to keep high accuracy in the interpolation procedure. Usually, these derivatives are computed in the spectral domain. A fast Fourier transform (FFT) algorithm is used to obtain the inverse Fourier transform. At every instant, the velocity and its derivatives should be transformed into the physical space. Regardless of the number of particles, 4 FFTs are required in the whole computational domain.

In the present study, a Hermite interpolation scheme using four points ( $N=4$ ) is extended in each direction without the additional FFT. When an arbitrary position of a particle  $(x, z)$  is located such that  $x_i \leq x \leq x_{i+1}$  and  $z_k \leq z \leq z_{k+1}$ , four points  $(x_{i-1}, \dots, x_{i+2})$  in the streamwise direction and four points  $(z_{k-1}, \dots, z_{k+2})$  in the spanwise direction are used in the interpolation. Therefore, data at 16 nearby grid points are used and the total information is 64 variables in the interpolation procedure for homogeneous directions. The corresponding basis functions can be specified as

$$\begin{aligned} H_1(\xi) &= (11\xi^7 - 52\xi^6 + 59\xi^5 + 50\xi^4 - 124\xi^3 \\ &+ 56\xi^2)/108, \\ H_2(\xi) &= (27\xi^7 - 81\xi^6 - 54\xi^5 + 270\xi^4 + 27\xi^3 \\ &- 297\xi^2)/108 + 1, \\ H_3(\xi) &= (-27\xi^7 + 108\xi^6 - 27\xi^5 - 270\xi^4 + 180\xi^3 \\ &+ 216\xi^2)/108, \\ H_4(\xi) &= (-11\xi^7 + 25\xi^6 + 22\xi^5 - 50\xi^4 - 11\xi^3 \\ &+ 25\xi^2)/108, \end{aligned} \quad (\text{A3})$$

$$\begin{aligned} G_1(\xi) &= (3\xi^7 - 15\xi^6 + 21\xi^5 + 3\xi^4 - 24\xi^3 + 12\xi^2)h/108, \\ G_2(\xi) &= (27\xi^7 - 108\xi^6 + 54\xi^5 + 216\xi^4 - 189\xi^3 \\ &- 108\xi^2)h/108 + h, \\ G_3(\xi) &= (27\xi^7 - 81\xi^6 - 27\xi^5 + 189\xi^4 - 108\xi^2)h/108, \\ G_4(\xi) &= (3\xi^7 - 6\xi^6 - 6\xi^5 + 12\xi^4 + 3\xi^3 - 6\xi^2)h/108, \end{aligned}$$

where  $\xi = (x - x_i)/h$  or  $\xi = (z - z_k)/h$  and  $h$  is the grid spacing.

- <sup>1</sup>G. I. Taylor, "Diffusion by continuous movements," *Proc. London Math. Soc.* **20**, 196 (1922).
- <sup>2</sup>A. S. Monin and A. M. Yaglom, *Statistical Fluid Mechanics* (MIT Press, Cambridge, MA, 1975).
- <sup>3</sup>S. B. Pope, "Lagrangian PDF methods for turbulent flows," *Annu. Rev. Fluid Mech.* **26**, 23 (1994).
- <sup>4</sup>P. K. Yeung and S. B. Pope, "Lagrangian statistics from direct numerical simulations of isotropic turbulence," *J. Fluid Mech.* **207**, 531 (1989).
- <sup>5</sup>P. K. Yeung, "One- and two-particle Lagrangian acceleration correlations in numerically simulated homogeneous turbulence," *Phys. Fluids* **9**, 2981 (1997).
- <sup>6</sup>N. Mordant, P. Metz, O. Michel, and J.-F. Pinton, "Measurement of Lagrangian velocity in fully developed turbulence," *Phys. Rev. Lett.* **87**, 214501 (2001).
- <sup>7</sup>A. La Porta, G. A. Voth, A. M. Crawford, J. Alexander, and E. Bodenschatz, "Fluid particle accelerations in fully developed turbulence," *Nature (London)* **409**, 1017 (2001).
- <sup>8</sup>P. K. Yeung, "Lagrangian investigations of turbulence," *Annu. Rev. Fluid Mech.* **34**, 114 (2002).
- <sup>9</sup>K. Kontomaris, T. J. Hanratty, and J. B. McLaughlin, "An algorithm for tracking fluid particles in a spectral simulation of turbulent channel flow," *J. Comput. Phys.* **103**, 231 (1992).
- <sup>10</sup>P. K. Yeung and S. B. Pope, "An algorithm for tracking fluid particles in numerical simulation of homogeneous turbulence," *J. Comput. Phys.* **79**, 373 (1988).
- <sup>11</sup>S. Balachandar and M. R. Maxey, "Methods for evaluating fluid velocities in spectral simulations of turbulence," *J. Comput. Phys.* **83**, 96 (1989).
- <sup>12</sup>Y. Sato and K. Yamamoto, "Lagrangian measurements of fluid-particle motion in an isotropic turbulent field," *J. Fluid Mech.* **175**, 183 (1987).
- <sup>13</sup>P. Vedula and P. K. Yeung, "Similarity scaling of acceleration and pressure statistics in numerical simulations of isotropic turbulence," *Phys. Fluids* **11**, 1208 (1999).
- <sup>14</sup>G. A. Voth, A. La Porta, A. M. Crawford, J. Alexander, and E. Bodenschatz, "Measurement of particle acceleration in fully developed turbulence," *J. Fluid Mech.* **469**, 121 (2002).
- <sup>15</sup>B. L. Sawford, "Reynolds number effects in Lagrangian stochastic models of turbulent dispersion," *Phys. Fluids A* **3**, 1577 (1991).
- <sup>16</sup>A. M. Reynolds, "A second-order Lagrangian stochastic model for particle trajectories in inhomogeneous turbulence," *Q. J. R. Meteorol. Soc.* **125**, 1735 (1999).
- <sup>17</sup>D. J. Thomson, "Criteria for the selection of stochastic models of particle trajectories in turbulent flow," *J. Fluid Mech.* **180**, 529 (1987).
- <sup>18</sup>J. D. Wilson and B. L. Sawford, "Review of Lagrangian stochastic models for trajectories in the turbulent atmosphere," *Boundary-Layer Meteorol.* **78**, 191 (1996).
- <sup>19</sup>S. Heinz, "On the Kolmogorov constant in stochastic turbulence models," *Phys. Fluids* **14**, 4095 (2002).
- <sup>20</sup>A. M. Reynolds, "On the application of nonextensive statistics to Lagrangian turbulence," *Phys. Fluids* **15**, L1 (2003).
- <sup>21</sup>R.-C. Lien and E. A. D'Asaro, "The Kolmogorov constant for the Lagrangian velocity spectrum and structure function," *Phys. Fluids* **14**, 4456 (2002).
- <sup>22</sup>K. D. Squire and J. K. Eaton, "Lagrangian and Eulerian statistics obtained from direct numerical simulations of homogeneous turbulence," *Phys. Fluids A* **3**, 130 (1991).
- <sup>23</sup>P. Shen and P. K. Yeung, "Fluid particle dispersion in homogeneous turbulent shear flow," *Phys. Fluids* **9**, 3472 (1997).
- <sup>24</sup>P. S. Bernard, M. F. Ashmawey, and R. A. Handler, "An analysis of particle trajectories in computer-simulated turbulent channel flow," *Phys. Fluids A* **1**, 1532 (1989).

- <sup>25</sup>P. S. Bernard and R. A. Handler, "Reynolds stress and the physics of turbulent momentum transport," *J. Fluid Mech.* **220**, 99 (1990).
- <sup>26</sup>A. Armenio, U. Piomelli, and V. Fiorotto, "Effect of the subgrid scales on particle motion," *Phys. Fluids* **11**, 3030 (1999).
- <sup>27</sup>M. R. Raupach and B. J. Legg, "Turbulent dispersion from an elevated line source: Measurements of wind-concentration moments and budgets," *J. Fluid Mech.* **136**, 111 (1983).
- <sup>28</sup>I. Iliopoulos and T. J. Hanratty, "Turbulent dispersion in a non-homogeneous field," *J. Fluid Mech.* **392**, 45 (1999).
- <sup>29</sup>A. M. Reynolds, "On the dynamical content of Lagrangian stochastic models in the well-mixed class," *Boundary-Layer Meteorol.* **103**, 143 (2002).
- <sup>30</sup>J. Kim, P. Moin, and R. Moser, "Turbulence statistics in fully developed channel flow at low Reynolds number," *J. Fluid Mech.* **177**, 133 (1987).
- <sup>31</sup>S. L. Lyons, T. J. Hanratty, and J. B. McLaughlin, "Large-scale computer simulation of fully developed turbulent channel flow with heat transfer," *Int. J. Numer. Methods Fluids* **13**, 999 (1991).
- <sup>32</sup>J. J. Riley and S. Corrsin, "The relation of turbulent diffusivities to Lagrangian velocity statistics for the simplest shear flow," *J. Geophys. Res.* **79**, 1768 (1974).
- <sup>33</sup>R. A. Antonia, T. Zhou, and G. P. Romano, "Second- and third-order longitudinal velocity structure functions in a fully developed turbulent channel flow," *Phys. Fluids* **9**, 3465 (1997).
- <sup>34</sup>K. R. Sreenivasan, "On the universality of the Kolmogorov constant," *Phys. Fluids* **7**, 2778 (1995).
- <sup>35</sup>B. L. Sawford and P. K. Yeung, "Lagrangian statistics in uniform shear flow: Direct numerical simulation and Lagrangian stochastic models," *Phys. Fluids* **13**, 2627 (2001).
- <sup>36</sup>B. W. Silverman, *Density Estimation for Statistics and Data Analysis* (Chapman & Hall, London, 1986).